

Interaction of Gold with a Pinwheel $\text{TiO}_{\sim 1.2}$ Film Formed on Rh(111) Facet: STM and DFT Studies

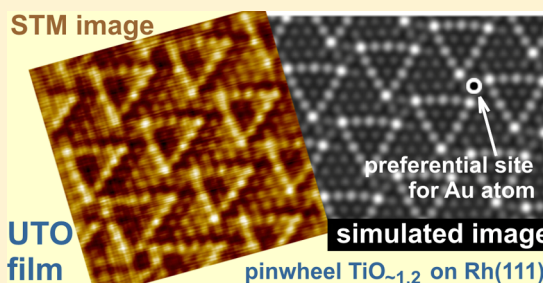
Pingo Mutombo,[†] Richárd Gubó,[‡] and András Berkó*,[§]

[†]Institute of Physics of Czech Academy of Sciences, Cukrovarnická 10, 162 00 Praha 6, Czech Republic

[‡]Department of Applied and Environmental Chemistry, University of Szeged, Rerrich Béla tér 1, 6720 Szeged, Hungary

[§]MTA-SZTE Reaction Kinetics and Surface Chemistry Research Group, Rerrich Béla tér 1, H-6720 Szeged, Hungary

ABSTRACT: The atomic structure of “pinwheel” $\text{TiO}_{\sim 1.2}$ ultrathin oxide (w-TiO-UTO) layer and its reaction with gold are studied by scanning tunneling microscopy (STM) imaging and density functional theory (DFT) calculations. The UTO film was formed as an encapsulation layer on the top facet (111) of stripe-like Rh nanoparticles supported on a $\text{TiO}_2(110)$ substrate. For proposing a structural model, the previous STM, photoelectron (XPS), and ion scattering spectroscopy (LEIS) results were also taken into account. DFT calculations were carried out within the generalized gradient approximation (GGA-PBE) in the frame of the Quantum Espresso code. A Rh(111) slab of four layers with a $\text{TiO}_{1.14}$ overlayer and a Rh–Ti–O stacking sequence were used. In the starting model, the ratio between hcp and fcc sites filled with Ti atoms was 1.54 (the same value for O atoms was 2.2) on the top of Rh layers. The simulation of the STM images of the relaxed structure was done following the Tersoff–Hamann approximation. The main structural characteristics obtained experimentally were successfully reproduced in the simulation results: (i) the chemical contrast appeared as a pinwheel structure and (ii) compared with an ideal hexagonal lattice, characteristic local distortions were found in the UTO film. In harmony with the experimental results, the DFT calculations of the adsorption of a single Au atom on a w-TiO-UTO layer indicated that there is a characteristic site preference within the unit cell of the UTO film. This feature was also experimentally demonstrated for the early stage of the deposition of Au at room temperature, suggesting a moderate template effect adjusted by the pinwheel structure. This work demonstrates clearly that the lack of the so-called “nanoholes” does not completely cancel the template effect because the periodic lattice strain in itself substitutes their role. Moreover, the weaker modulation of Au/TiO-UTO bond permits the formation of one atomic layer thick 2D gold nanoparticles at 300 K.



INTRODUCTION

Long-range ordered ultrathin oxide (UTO) films formed in a completely oxidized or a partially reduced form with determined stoichiometry are recently the subject of intensive experimental and theoretical work.^{1–4} The interest toward ultrathin films (oxide, covalent, or metal) derives from their unexpected structural and electronic properties that are completely different with respect to their bulk counterparts. Moreover, the huge interest for these films not only originates from fundamental aspects but also connects to the technological importance of the fabrication of different supported or self-supporting 2D materials like oxides, graphene, dichalcogenides, or polymers.^{1,3,5–7} Concerning the UTO films, they usually possess charge distribution balanced via strained atomic positions, which is also controlled by the substrate supporting them. The result is a periodic supercell (2 to 3 nm) structure making these films excellent candidates as templates.^{8–10} This latter topic connects to the nanotechnology concept previously described using UTO films as nanotemplates for tailored growth of metal nanoparticles. Although, the controlled growth of the UTO films on different metal surfaces is not a new idea, nevertheless, it became possible only recently that the

formation of an epitaxial oxide film can be followed on an atomic scale by scanning probe microscopy (SPM) techniques.^{1,2,4} The results obtained in the past decade obviously led to a successful synthesis of the findings.^{11–13} The most indicative parameter used for the characterization of UTO films is the oxidation state of the cation and the wetting ability of the oxide layer on different support metals. In general, the low oxidation state results in a high wetting ability and the appearance of unusual patterns like “wheel” or “zig-zag” structures.^{4,11,14–28} Different explanations were suggested for the appearance of these STM patterns: (i) some extent of alloying of the substrate metal atoms in the UTO overlayer;^{16,29} (ii) formation of stacking faults of reversed metal–oxygen positions (O or M termination of the double layer);¹⁸ (iii) building of extra oxygen atoms in a periodic manner in the O-terminated M–O double layer causing some (10–20%) increase in the Ti:O = 1 stoichiometry; the supercell periodicity is controlled by the misfit of the supporting metal lattice and that

Received: April 19, 2016

Revised: May 19, 2016

Published: May 20, 2016

of the UTO film.^{11,20} The most detailed experimental work has been performed on Pt(111) surface to explore all different ordered TiO_x phases as a function of the preparation conditions (O_2 pressure, temperature, metal deposition rate).²² Sedona et al. provided a detailed discussion on this issue in the light of bond strength of the different constituents of the substrate/UTO-overlayer system. In another paper they collected and analyzed the special “wheel” (w) structures (supercell) and concluded that a simple moiré-model seems to explain a wealth of experimental data, but probably a complete quantum mechanical calculation is needed to provide the structural details within the supercell.²³ Several steps in this direction have already been made.^{11,21,24,26} On the basis of these studies, we used an appropriate model in this work for obtaining simulated STM images reflecting the main features observed by STM for the $\text{TiO}_2(110)/\text{Rh}(111)/\text{w-TiO}_{\sim 1.2}$ -UTO decoration system.^{27,28,30,31} Moreover, we tested both experimentally the adsorption of gold at the low coverage limit and theoretically the bonding of a single gold atom at the different sites of a $\text{w-TiO}_{\sim 1.2}$ -UTO film.

EXPERIMENTAL AND COMPUTATIONAL DETAILS

The scanning tunneling microscopy (STM) images of 256×256 pixels presented in this work were recorded by a commercial room temperature (RT) scanning tunneling microscope (WA-Technology) built in a conventional UHV system, which was also equipped by a 4-pocket e-beam metal evaporator (Oxford Instruments) for deposition of Rh and Au, a quadrupole mass spectrometer (Balzers), and an Auger-electron spectrometer (Staib DP-CMA). The cleaning procedure of $\text{TiO}_2(110)$ surfaces, the preparation of encapsulated Rh nanocrystallites, and the calibration of STM for the nanoscale distances are described in detail elsewhere.^{27,28} The STM imaging was performed in both constant current (cc) and constant height (ch) modes. The typical cc-imaging parameters of $U_{\text{bias}} = +1.5$ V (in respect to the sample) and $I = 0.1$ nA were applied. The deposition of Rh and Au was carried out at a rate of ~ 0.5 ML/min.

DFT calculations were carried out within a generalized gradient approximation (GGA-PBE), as implemented in the Quantum Espresso code.³² We employed ultrasoft pseudopotentials and plane-wave basis set.³³ The Rh and the O atoms were described by a $4d^8 5s^1$ and a $2s^2 p^4$ electron configurations, respectively. The Ti pseudopotential has a $3s^2 3p^6 4s^2 3d^2$ configuration including the 3s, 3p semicore states. For Au, a $5d^{10} 6s^1 6p^0$ electronic configuration was used. The cutoff energies for the expansion of the plane-wave basis set and the electronic density were set to 30 and 300 Ry, respectively. We used a k-point set of $2 \times 2 \times 1$ for the integration in the Brillouin-zone. In executing the consecutive calculation cycles, the convergence was considered achieved when the total energy difference was smaller than 0.3 mRy and the difference of the atomic forces remained below 0.1 mRy/Bohr.

For the construction of an appropriate structural model, the unit-cell Wood-matrix ($a_{11} = 7$; $a_{12} = 5$; $a_{21} = 2$; $a_{22} = 7$) with respect to the Rh(111) surface with cell vectors equal to 1.7089 nm was used, similarly as in the model described for encapsulation TiO_x pinwheel layers formed on (111) top facets of supported Pd nanoparticles.¹⁷ Note that in contrast with the structural model proposed in that paper in which the surface is terminated by Ti ions, in the present work an M–Ti–O stacking was considered. The Rh (111) slab has four layers with Rh–Rh first neighbor corresponding to 0.2736 nm. To

separate the slabs in the direction perpendicular to the surface, we used a vacuum layer of 1.2 nm. All of the atoms of the supercell were allowed to relax except the two bottom Rh layers. To study the interaction of w-TiO -UTO layer with a metallic species, we placed a single gold atom on the adsorption sites of the relaxed structure (see below), as indicated in Figure 4: on top of Ti atoms of Ti_4 (Top_4) and Ti_3 (Top_3), on the top of oxygen atom (Top_O), among the Ti_4 atoms and oxygen atoms (H_4), among the Ti_3 atoms and oxygen atoms (H_6), and at the hollow site among the bright triangles (H_9). Moreover, we also calculated the change in energy connected to a possible exchange between the Ti_4 or Ti_3 atoms with an Au atom. To determine the change in the electronic structure of the surface upon gold adsorption, we calculated the projected density of states (PDOS) and simulated STM images of both the w-TiO -UTO layer and the best Au/ w-TiO -UTO surface configuration. Note that these simulations were done following the Tersoff–Hamann approximation, which assumes that the STM current is proportional to the local density of states.³⁴ STM maps were calculated at 1.8 V and at a height corresponding to 0.32 nm above the surface.

RESULTS AND DISCUSSION

STM Measurements. The reproducible formation of a pinwheel ultrathin $\text{TiO}_{\sim 1.2}$ film (w-TiO -UTO) on extended (111) top facet of supported Rh nanoparticles was described in our previous works.^{27–31} In short, ~ 10 ML (monolayer) Rh was deposited on a clean $\text{TiO}_2(110)$ surface at RT, followed by 10 min annealing at 1050 K. After several cycles of the latter thermal treatments, large-area 20–30 atomic layer thick Rh nanoparticles (bright regions in the constant current STM image) are formed with one edge parallel to [001] crystallographic orientation of the $\text{TiO}_2(110)$ support due to a dewetting process above 950 K (Figure 1a). This observation is very important because it indicates the direction of the Rh(111) lattice, which is not detectable immediately by STM

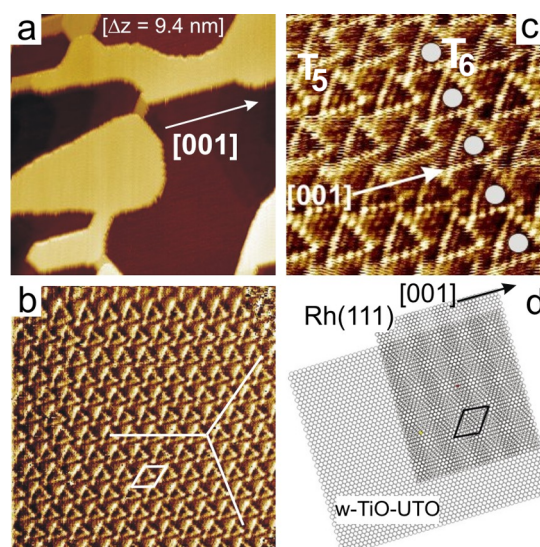


Figure 1. (a) STM cc-image of $200 \times 200 \text{ nm}^2$ taken on a $\text{TiO}_2(110)$ surface decorated by Rh multilayer nanostructures possessing flat Rh(111) top facet decorated by $\text{TiO}_{\sim 1.2}$ ultrathin film. STM ch-images of (b) $20 \times 20 \text{ nm}^2$ and (c) $8 \times 8 \text{ nm}^2$ recorded on the decorated top facet. (d) Moiré pattern formed by superposition of Rh(111) and w-TiO -UTO hexagonal lattices.

due to the covering w-TiO-UTO film. Note that the shape of the particles will gradually become more compact (usually of hexagonal outline) as an effect of repeated thermal treatments. The constant height STM image of $20 \times 20 \text{ nm}^2$ recorded on the top facet of a Rh nanoparticle shows a highly ordered phase (Figure 1b). Although the periodicity of the structure is almost perfect, the larger resolution image of $8 \times 8 \text{ nm}^2$ reveals two different characteristic triangles consisting of five or six dots (T5, T6). In the present case, the T5 form is the typical one and the position of the T6 forms (indicated by gray circles) suggests a 1D phase boundary character (Figure 1c). The main crystallographic orientations and the supercell area are drawn in Figure 1b. The characteristic periodicity length of $1.66 (\pm 0.05) \text{ nm}$ was determined for the hexagonal supercell. This value is slightly higher than that given in our first work devoted to the same system,²⁷ nevertheless, the present value can be considered as a more precise one. The hexagonal lattice constant determined by both the brighter and darker dots is $0.32 (\pm 0.01) \text{ nm}$. These dots can be identified with Ti ions of the w-TiO-UTO film (Figure 1c). A further important parameter is the slight rotation between the close-packed direction of the w-TiO-UTO overlattice and the Rh(111) support (the top facet of the Rh nanocrystallites). In the case of the latter lattice, as previously mentioned, the [001] orientation of the $\text{TiO}_2(110)$ surface is an appropriate direction that can be easily determined. Accordingly, a rotation of 2 to 3 grad was measured between the Rh and the oxide overlayer lattice. All of these morphological data can be fitted together in the frame of a moiré construction using two lattices with a unit vector of 0.269 nm – Rh(111) – and another one of 0.32 nm – w-TiO-UTO – which are rotated by $\sim 2 \text{ grad}$ (Figure 1d). As can be seen, this simple combined texture provides a clear appearance of a supercell whose size ($\sim 1.7 \text{ nm}$) is very close to the periodicity of the pinwheel structure described above. This result leads to the conclusion that the misfit of the two lattices immediately determines the long-range structural wave of the metal/UTO system. Nevertheless, a “classic” moiré pattern can be obtained only in the case of a completely oxidized overlayer like an epitaxial TiO_2 film on Ru(0001).³⁵ To explain the large chemical contrast between the adjacent Ti ions in our case, we need to assume a special chemical and structural composition of the layer. Regarding very strong XPS evidence^{28,30} for the O:Ti stoichiometry exceeding 1 by 10–20% and taking into account some previous successful theoretical simulations,^{11,21,24,26} we present below a DFT calculation for a model structure explaining the STM images recorded on Rh(111) facets decorated by w-TiO-UTO film.

To complete the recent studies on 2-D $\text{Au}(\text{Rh}, \text{Pd})/\text{TiO}_x$ -UTO model systems^{28,30,31,36,37} and to support the DFT calculations presented in this work, we investigated the adsorption of gold on a w-TiO-UTO film at the low-coverage regime. Note that in contrast with our previous work³¹ where a higher temperature (400–500 K) of the substrate was applied during Au deposition, in the present study we used the lowest temperature ($300 \pm 5 \text{ K}$) attainable in our measurement system. Because of this low substrate temperature, the gold formed one-atom-thick 2D crystallites sitting on the top of the oxide film in agreement with the theoretical calculation described below. Unlike our previous study performed at higher temperature (500 K), probably no exchange between the gold and the oxide layer took place. The STM image of $20 \text{ nm} \times 20 \text{ nm}$ in Figure 4c shows a w-TiO-UTO film exposed at 300 K by ~ 0.1 monolayer (ML) of gold. The height of the

nanoparticles is $\sim 0.2 \text{ nm}$, the diameter of them changes in the range of 1.5 to 2 nm, the particle size distribution is very narrow, and the position of the particles exhibits a clear ordering (Figure 4e). These properties are characteristic for nanoparticles grown and templated on the top of TiO_x -UTO film.⁹ Note that the surface concentration of the nanoparticles is $\sim 1.3 \times 10^{12} \text{ cm}^{-2}$ which is only two to three times higher than the value received for Rh-free regions of $\text{TiO}_2(110)$ surface shown in Figure 1a. The neighboring particles are in a distance of $\sim 1.6 \text{ nm}$ very close to the unit cell vector of the wheel structure (Figure 4c,e). The constant height image in Figure 4d exhibits a single Au particle of a sufficiently small size to clearly detect that the pinwheel structure circumvented the particle. As indicated by straight lines, the Au nanoparticle consists of approximately six to eight atoms centered almost perfectly in the region among the corners of three bright triangles (H_3 site as denoted below). This finding is in excellent agreement with the prediction of DFT calculations presented in the following chapter.

DFT Calculations. As previously mentioned, the w-TiO-UTO layer was modeled with M–Ti–O stacking sequence proposed by Barcaro et al.,¹¹ where “M” refers to Rh in our case. Note that the mechanism widely accepted for the formation of an encapsulation layer on a supported metal nanoparticle is based on the diffusion of Ti and O atoms of the bulk to the Rh(111) top facets and the occupation of fcc or hcp sites. The diffusion of oxygen on top of titanium layer (formation of O-terminated UTO film) is thermodynamically favored because of the larger heat of formation of Ti–O ($672 \pm 9.2 \text{ kJ/mol}$) than Rh–O ($405 \pm 41.8 \text{ kJ/mol}$) bond. Figure 2a

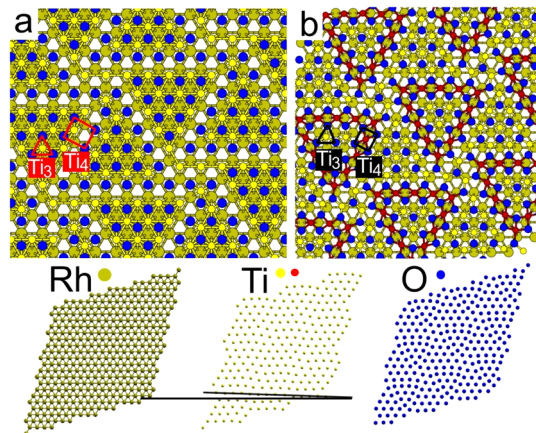


Figure 2. (a) Initial and (b) relaxed atomic positions of the w-TiO-UTO layer. (For more details, see the text.) At the bottom of the figure the relaxed atomic layer structure of the different elements (Rh, Ti, O) can be seen.

shows the atomic ball model we have used to describe the w-TiO-UTO layer, where the Ti and O atoms are placed in hcp/fcc sites on the Rh(111) surfaces in such a way that the periodicity criterion be fulfilled and a Ti:O = 1.14 stoichiometry is obtained. Note that because of lattice mismatch between the substrate (0.270 nm) and TiO layer (0.315 nm), dislocations lines are formed. Therefore, Ti atoms inside the islands are 3-fold coordinated (Ti_3) to O atoms, while those at the boundary are constructed as 4-fold O-coordinated (Ti_4) sites (Figure 2a). The number of Ti and O atoms placed in the fcc/hcp sites were 17/11 and 22/10, respectively. The atomic model of the w-

TiO-UTO layer previously described corresponds to the so-called T5 structure (Figure 3b).²⁸ Note that to simulate the T6

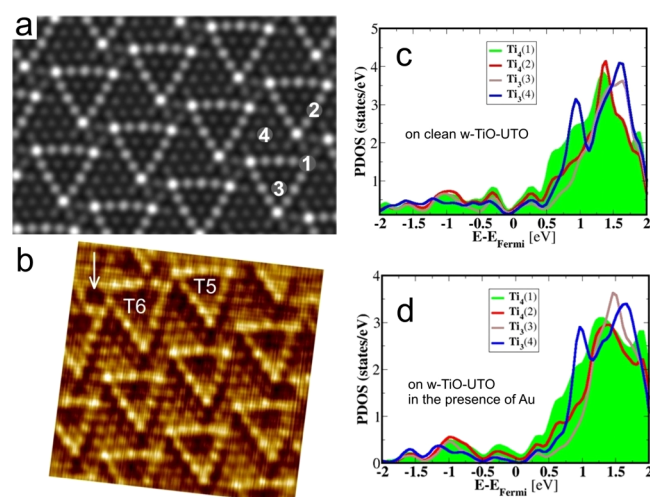


Figure 3. (a) Simulated and (b) measured STM ch-images ($5 \times 5 \text{ nm}^2$) for comparison of the lattice distortions. The projected density of empty states (PDOS) of selected Ti ions for (c) a clean and (d) a single Au-atom-decorated (see the text) w-TiO-UTO layer.

structure mentioned above, the number of Ti and O atoms found in the fcc/hcp sites was modified to 22/6 and 17/15, respectively. Performing the DFT calculations described above, it was found that upon structural relaxation the Ti_4 and Ti_3 ions belonging to the brighter triangular islands detected by STM have the same height (Figures 2b and 3b). On average, they lie above the Rh topmost layer by 0.220 nm. Furthermore, the average height of the remaining Ti_3 cations (those located outside the brighter triangle) was $\sim 0.216 \text{ nm}$ above the same Rh layer. This suggested that the vertical separation between the two kinds of islands was $\sim 0.004 \text{ nm}$. A similar trend was also obtained upon the relaxation of T6 structure (not shown), except that a few Ti ions located at the borderline of the islands moved up or down (two atoms relaxed up by 0.001 nm and two others relaxed down by 0.002 nm with respect to the average position of Ti ions in the brighter triangle. The lateral position of Ti and O ions of the relaxed structure is shown in Figure 2 (bottom). It was found that the oxygen layer is strongly distorted, especially along the dislocation line; moreover, the average position of the O layer is located 0.285 nm above the topmost Rh layer. It is clear that the Ti ions also exhibit a strong local deviation from the approximate direction of the atomic rows, which are in a rotated position of 3 grad relative to the original Rh(111) close-packed direction. Accordingly, the STM observation of a slight rotation between Rh(111) and w-TiO-UTO lattices is automatically reflected via the calculations.²⁷

The simulation of STM images was done following the Tersoff–Hamann approximation, which assumes that the STM current is proportional to the local density of states.³⁴ Maps were simulated at 1.8 V and at a height corresponding to 0.32 nm above the topmost oxygen atom (Figure 3a). It should be pointed out that at positive bias voltage, the densities of state above the Fermi level are dominated by the d-orbitals of the Ti ions, so the dots appearing in STM images correspond to Ti ions. It is obvious at first glance that the simulated and the measured STM images for the T5 pattern agree very well (Figure 3a,b): (i) formation of triangles consisting of five dots;

(ii) higher brightness at the corner dots; (iii) all sites of the hexagonal lattice are visible (there is no missing Ti ion, “pico-hole”); (iv) comparing the experimental and the calculated images, the deviation of the dots (brighter or darker) from an ideal hexagonal lattice is well reproduced. It is important to note that although a picohole-like feature at the corner of the triangles was found in the STM-simulated image for the T6 structure, no Ti cation was missing even in that case. This nanohole feature is simply the result of a downward relaxation of one of the Ti ions among corner Ti ions of the triangles, which is located 0.02 nm below the average Ti layer. We found that the Ti_4 atoms appear brighter than Ti_3 ions; furthermore, the corner Ti_4 ions look the brightest. It is also an important result that after the relaxation the Ti_4 atoms are in 2-fold Rh-bridge positions, indicated by red circles in Figure 2b. Because all Ti ions of the brighter triangular islands have more or less the same height, the difference in the atomic contrast can be ascribed to electronic effects. To verify this idea, we computed the projected density of states of some characteristic atoms labeled 1, 2, 3, and 4 in Figure 3a and integrated the area under the PDOS curves from Fermi energy to +2.0 eV (Figure 3c). The results are shown in Table 1. It can be seen that the corner

Table 1. Integrated Values from Fermi Energy to +2.0 eV under the PDOS Curves (Empty Electronic States) and Lowdin Atomic Charges Taken for Different Ti Ion Positions Calculated for a Clean ($E_f = 6.211 \text{ eV}$) and an Au-Decorated ($E_f = 3.4892 \text{ eV}$) w-TiO-UTO Layer^a

position of Ti ion (see Figure 3a)	empty electronic states (e^-) (w-TiO-UTO)	Lowdin atomic charge (e^-) (w-TiO-UTO)	Lowdin atomic charge (e^-) Au on w-TiO-UTO
1	3.97	10.718	10.710
2	3.34	10.736	10.735
3	3.18	10.730	10.729
4	3.79	10.772	10.771

^aCorresponding PDOS curves are shown in Figure 3c,d.

$\text{Ti}_4(1)$ has a higher number of electronic states than $\text{Ti}_4(2)$. This explained why the corner Ti_4 looks brighter than the other Ti_4 ions in STM images. Moreover, $\text{Ti}_3(3)$ exhibits a lower number of states than $\text{Ti}_3(4)$ atom. Because the latter site lies by 0.004 nm with respect to the other site (see above), its darker appearance is probably connected to the geometrical factor. On the basis of DFT total energy calculations, it is found that the T5 structure is energetically lower than the T6 model by 1.03 eV. This makes the formation of the latter structure unlikely at low temperature. But because the w-TiO-UTO film is formed after repeated cycles of thermal annealing, the energy barrier for its formation of the T6 structure can be overcome. This can explain the rare occurrence of T6 structure in STM experimental findings with respect to T5.²⁸

We estimated the adhesion energy of the oxide layer on the Rh(111) surface by separately calculating the total energy of the relaxed Rh(111) surface (E_1), the relaxed oxide layer (E_2), and the oxide/Rh(111) system (E_3). The energy of adhesion E_{ad} was then determined as $E_{ad} = [(E_1 + E_2) - E_3]/A$, where A indicates the surface area. All calculations were carried out using the same supercell as mentioned above. We found out that the adhesion energy equals 28.3 eV/nm^2 (4.534 J/m^2), suggesting a strong adhesion of the w-TiO-UTO film at the Rh(111) surface. The formation of strong covalent bonds at the interface

between the oxide film and the Rh surface leads to a higher stability (or a very low reactivity) of the oxide film.

In the following part we analyze our DFT results obtained by putting an Au atom on the different sites of the w-TiO-UTO layer listed in Table 2 and indicated in Figure 4a. The DFT

Table 2. Total Energy Differences (eV) with Respect to the Best Adsorption Site (H_9) for a Single Gold Atom Decorated w-TiO-UTO Super Cell

adsorption site	brighter triangle	darker triangle
H_9	0	0
Top_4 , H_4	0.23	0.23
Top_3 , H_6	0.29	0.24
Top_O	0.65	0.66
Exchange- Top_4	1.05	
Exchange- Top_3		3.08

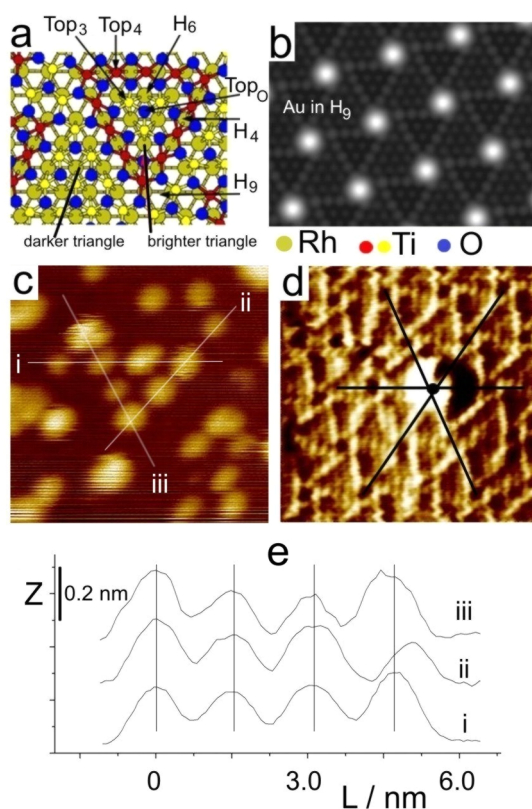


Figure 4. (a) Adsorption sites for Au atom used in the DFT calculations. (b) STM simulation of Au adsorbed at the H_9 site on the TiO-UTO surface. (c) STM cc-image of $10 \times 10 \text{ nm}^2$ taken on w-TiO-UTO film deposited by Au of $<0.005 \text{ ML}$ at 300 K. (d) STM ch-image of $7 \times 7 \text{ nm}^2$ showing the position of an Au nanocluster consisting of six to eight Au atoms relative to the wheel structure. (e) z profiles taken along the lines indicated in panel c.

total energy calculations suggest that the best adsorption site for gold is the H_9 position, which was chosen as a reference point in Table 2. In this position Au atom lies above the average Rh topmost layer by 0.518 nm, and it is bonded in top configuration to a Ti atom positioned at the intercorner region of the bright triangles. The calculated Au–Ti bond length equals 0.253 nm. We calculated the adsorption energy by subtracting the energy of the relaxed w-TiO-UTO/Rh(111) surface and of the isolated Au atom from the total energy of the

system and by considering the absolute value. The adsorption energy of Au at the H_9 site is 2.72 eV. This value is slightly lower than what was found for a gold atom at the “k-TiO_x” phase of the Au/TiO_x/Pt(111) system (2.96 eV), where the Au gets trapped in nanoholes, but it is certainly higher than those values found for other phases such as “rect”, “z-TiO_x”, and “z'-TiO_x”.^{38,39} Although the added gold does not induce a great change in the atomic geometry of the surface oxide film, the surrounding oxygen atoms are affected rather strongly. They move down by 0.005 nm. By putting Au atom in all other positions calculated here, the total energy increases. The calculation of Au in Top_4 and H_4 sites leads to a total energy that is higher by 0.23 eV for both sites. Moreover, we found that in the case of Au at the Top_3 or H_6 sites the total energy increases for the brighter triangle and darker triangle by 0.29 and 0.24 eV, respectively (Table 2). This indicates a different reactivity of Au with respect to these islands; the gold atom prefers rather to adsorb at the Top_3 or H_6 sites located at the darker triangle instead of the brighter one. The occupation of Au on top of an oxygen atom (Top_O) results in an even larger total energy increase compared with H_9 site (reference point). In contrast with the Top_3 sites, the reactivity of Au to oxygen atoms of both triangles is about the same. Furthermore, it was found that placing Au in the H_4 and H_6 sites results in unstable configurations. For both initial configurations, Au moves from the H_4 (H_6) sites to the Top_4 (Top_3) positions, suggesting a very low energy barrier between these sites (H_4 – Top_4 , H_6 – Top_3).

Regarding the possible exchange between the Au and the Ti atoms located in Top_4 (Top_3), our calculations suggest that such possibilities are unlikely owing to high energy difference (Table 2). This means that Au is more likely to be found on top of the w-TiO-UTO layer than at the oxide/Rh interface. Note that in a previous experimental work a significant exchange between Ti and added Rh was observed only above 250 K sample temperature, and it was concluded that this process is thermally activated.³⁷ For gold, similar exchange behavior was detected at $>500 \text{ K}$.³¹ In the present work we found that the gold grows on the top of the UTO film at RT and a well detectable template effect was observed (see above).

We have also calculated the projected densities of state of selected Ti atoms in the presence of an Au atom at H_9 site (Figure 3d). We followed the same procedure for the same atomic sites considered above in the case of a clean w-TiO-UTO surface. It is worth mentioning that the presence of Au caused only a slight modification of the density of empty states. This finding is further correlated with the fact that the Lowdin atomic charges of the same atoms before and after Au adsorption, as shown in the Table 1, are almost the same. Moreover, the Lowdin charge of the Au atom shows an increase in the number of electrons by $0.54e^-$. Thus, there is an overall charge transfer from the slab to Au atom. Most of the electrons transferred come from the Ti atom bonded to Au and from the nearby O atoms. All other atoms of the slab give only a tiny part of their electronic charge. The simulated STM image (1.8 V, 0.32 nm above w-TiO-UTO surface) is displayed in Figure 4b. Gold appears as a bright protrusion at the regions among the corners of the bright triangles (around H_9 site). The STM contrast of Au is mostly due to its atomic height above the surface (0.518 nm above the Rh surface, i.e., 0.3 nm above the topmost Ti atoms). Interestingly, it is still possible to make a distinction between the brighter and darker islands even upon the adsorption of Au. One can suggest that both topographic

and electronic effects play a great role in the appearance of STM images of the Au/w-TiO-UTO interface. It is also worth remarking that the negative charge of gold atoms adsorbed in H_9 sites probably also contributes to the appearance of the template effect observed by STM (see above).

CONCLUSIONS

In the first part of this work we presented shortly an experimental procedure by which extended Rh nanoparticles possessing large (111) top facets and encapsulated by pinwheel $TiO_{x-1.2}$ UTO layer can easily and reproducibly be fabricated. The atomic level structure of the highly ordered w-TiO-UTO decoration layer was revealed by STM. Taking into account the structural/spectroscopic data and predictions of similar UTO layers described in the last several years for several other material compositions, the structural relaxation of a simply constructed initial atomic configuration was tested by DFT calculations. The relaxed structure was used for simulating STM images. It was found that the simulated image fits well to the STM image recorded in constant height mode. The lateral distortion of Ti ion layer from an ideal hexagonal lattice and the relative brightness of the different Ti sites reflect themselves perfectly in the simulated images. The results clearly show that the characteristic “pinwheel” pattern (consisting of bright triangles) is mainly a consequence of the O:Ti stoichiometry exceeding 1 and of the different oxygen coordination of the individual Ti ions within the supercell. The two variants of the wheel structures (T5 and T6) of the same size supercell found by STM were well reproduced via the simulations. The DFT calculations clearly showed that strong covalent bonds form at the interface between the oxide film and Rh surface, leading to an increased stability and a very low reactivity of the oxide film. Au atom was found to be adsorbed preferentially at the intercorner region among the bright triangles of the pinwheel pattern. It was shown also by STM measurements that the initial nucleation of gold proceeds preferentially at these sites at RT, and a clear evidence was found for a template-governed growth of gold at 300 K. The theoretical calculations suggested that there is a charge rearrangement within the layer on the effect of Au adsorption; moreover, looking at Lowdin charge of Au atom, an overall charge transfer ($0.54 e^-$) from the slab to Au was found.

AUTHOR INFORMATION

Corresponding Author

*E-mail: aberko@chem.u-szeged.hu. Tel: 00 36 62 544 646.

Notes

The authors declare no competing financial interest.

ACKNOWLEDGMENTS

Access to computing and storage facilities owned by parties and projects contributing to the National Grid Infrastructure MetaCentrum (Czech Republic), provided under the program “Projects of Large Infrastructure for Research, Development, and Innovations” (LM2010005), is greatly appreciated. The financial support of the OTKA project NN 110676 (National Research, Development and Innovation Office, Hungary) is acknowledged. We are thankful for the support of EU-COST Action CM1104 and for the enjoyable and fruitful discussions with Dr. László Óvári, Dr. László Deák, and Dr. Martin Ondráček.

REFERENCES

- (1) Freund, H.-J.; Pacchioni, G. Oxide Ultra-thin Films on Metals: New Materials for the Design of Supported Metal Catalysts. *Chem. Soc. Rev.* **2008**, *37*, 2224–2242.
- (2) Nilus, N. Properties of Oxide Thin Films and their Adsorption Behavior Studied by Scanning Tunneling Microscopy and Conductance Spectroscopy. *Surf. Sci. Rep.* **2009**, *64*, 595–659.
- (3) Pacchioni, G. Two-Dimensional Oxides: Multifunctional Materials for Advanced Technologies. *Chem. - Eur. J.* **2012**, *18*, 10144–10158.
- (4) Surnev, S.; Fortunelli, A.; Netzer, F. P. Structure-Property Relationship and Chemical Aspects of Oxide-Metal Hybrid Nanostructures. *Chem. Rev.* **2013**, *113*, 4314–4372.
- (5) Bae, S.; Kim, H.; Lee, Y.; Xu, X.; Park, J.-S.; Zheng, Y.; Balakrishnan, J.; Lei, T.; Kim, H. R.; Song, Y. I.; et al. Roll-to-roll Production of 30-in. Graphene Films for Transparent Electrodes. *Nat. Nanotechnol.* **2010**, *5*, S74–S78.
- (6) Wang, Q. H.; Kalantar-Zadeh, K.; Kis, A.; Coleman, J. N.; Strano, M. S. Electronics and Optoelectronics of Two-dimensional Transition Metal Dichalcogenides. *Nat. Nanotechnol.* **2012**, *7*, 699–712.
- (7) Colson, J. W.; Dichtel, W. R. Rationally Synthesized Two-dimensional Polymers. *Nat. Chem.* **2013**, *5*, 453–465.
- (8) Gavioli, L.; Cavaliere, E.; Agnoli, S.; Barcaro, G.; Fortunelli, A.; Granozzi, G. Template-assisted Assembly of Transition Metal Nanoparticles on Oxide Ultrathin Films. *Prog. Surf. Sci.* **2011**, *86*, 59–81.
- (9) Breinlich, C.; Buchholz, M.; Moors, M.; Pertram, T.; Becker, C.; Wandelt, K. Distribution of Pd Clusters on Ultrathin, Epitaxial TiO_x Films on $Pt_3Ti(111)$. *Beilstein J. Nanotechnol.* **2015**, *6*, 2007–2014.
- (10) Schmid, M.; Kresse, G.; Buchsbaum, A.; Napetschnig, E.; Gritschneider, S.; Reichling, M.; Varga, P. Nanotemplate with Holes: Ultrathin Alumina on $Ni_3Al(111)$. *Phys. Rev. Lett.* **2007**, *99*, 196104.
- (11) Barcaro, G.; Cavaliere, E.; Artiglia, L.; Sementa, L.; Gavioli, L.; Granozzi, G.; Fortunelli, A. Building Principles and Structural Motifs in TiO_x Ultrathin Films on a (111) Substrate. *J. Phys. Chem. C* **2012**, *116*, 13302–13306.
- (12) Barcaro, G.; Agnoli, S.; Sedona, F.; Rizzi, G. A.; Fortunelli, A.; Granozzi, G. Structure of Reduced Ultrathin TiO_x Polar Films on $Pt(111)$. *J. Phys. Chem. C* **2009**, *113*, 5721–5729.
- (13) Pacchioni, G.; Freund, H.-J. Electron Transfer at Oxide Surfaces. The MgO Paradigm: from Defects to Ultrathin Films. *Chem. Rev.* **2013**, *113*, 4035–4072.
- (14) Diebold, U. The surface Science of Titanium Dioxide. *Surf. Sci. Rep.* **2003**, *48*, 53–229.
- (15) Wu, C.; Marshall, S. J.; Castell, M. R. Surface Structures of Ultrathin TiO_x Films on $Au(111)$. *J. Phys. Chem. C* **2011**, *115*, 8643–8652.
- (16) Bowker, M.; Stone, P.; Morrall, P.; Smith, R.; Bennett, R.; Perkins, N.; Kvon, R.; Pang, C.; Fourre, E.; Hall, M. Model Catalyst Studies of the Strong Metal–Support Interaction: Surface Structure Identified by STM on Pd Nanoparticles on $TiO_2(110)$. *J. Catal.* **2005**, *234*, 172–181.
- (17) Bennett, R. A.; Pang, C. P.; Perkins, N.; Smith, R. D.; Morrall, P.; Kvon, R. I.; Bowker, M. Surface Structures in the SMSI State: Pd on (1×2) Reconstructed $TiO_2(110)$. *J. Phys. Chem. B* **2002**, *106*, 4688–4696.
- (18) Dulub, O.; Hebenstreit, W.; Diebold, U. Imaging Cluster Surfaces with Atomic Resolution: The Strong Metal-Support Interaction State of Pt Supported on $TiO_2(110)$. *Phys. Rev. Lett.* **2000**, *84*, 3646–3649.
- (19) Pang, C. L.; Lindsay, R.; Thornton, G. Structure of Clean and Adsorbate-Covered Single-Crystal Rutile TiO_2 Surfaces. *Chem. Rev.* **2013**, *113*, 3887–3948.
- (20) Schoiswohl, J.; Sock, M.; Eck, S.; Surnev, S.; Ramsey, M. G.; Netzer, F. P.; Kresse, G. Atomic-level Growth Study of Vanadium Oxide Nanostructures on $Rh(111)$. *Phys. Rev. B: Condens. Matter Phys.* **2004**, *69*, 155403–155413.
- (21) Schoiswohl, J.; Surnev, S.; Sock, M.; Eck, S.; Ramsey, M. G.; Netzer, F. P.; Kresse, G. Reduction of Vanadium-oxide Monolayer

Structures. *Phys. Rev. B: Condens. Matter Mater. Phys.* **2005**, *71*, 165437–165444.

(22) Sedona, F.; Rizzi, G. A.; Agnoli, S.; Llabrés i Xamena, F. X.; Papageorgiou, A.; Ostermann, D.; Samb, M.; Finetti, P.; Schierbaum, K.; Granozzi, G. Ultrathin TiO_x Films on Pt(111): A LEED, XPS, and STM Investigation. *J. Phys. Chem. B* **2005**, *109*, 24411–24426.

(23) Sedona, F.; Agnoli, S.; Granozzi, G. Ultrathin Wagon-Wheel-like TiO_x Phases on Pt(111): A Combined Low-Energy Electron Diffraction and Scanning Tunneling Microscopy Investigation. *J. Phys. Chem. B* **2006**, *110*, 15359–15367.

(24) Wu, Q.-H.; Fortunelli, A.; Granozzi, G. Preparation, Characterisation and Structure of Ti and Al Ultrathin Oxide Films on Metals. *Int. Rev. Phys. Chem.* **2009**, *28*, 517–576.

(25) Zhang, L. P.; vanEk, J.; Diebold, U. Spatial Self-Organization of a Nanoscale Structure on the Pt(111) Surface. *Phys. Rev. B: Condens. Matter Mater. Phys.* **1999**, *59*, 5837–5846.

(26) Zhang, Y.; Giordano, L.; Pacchioni, G.; Vittadini, A.; Sedona, F.; Finetti, P.; Granozzi, G. The Structure of a Stoichiometric TiO_2 Nanophase on Pt(111). *Surf. Sci.* **2007**, *601*, 3488–3496.

(27) Majzik, Z.; Balázs, N.; Berkó, A. Ordered SMSI Decoration Layer on Rh Nanoparticles Grown on $\text{TiO}_2(110)$ Surface. *J. Phys. Chem. C* **2011**, *115*, 9535–9544.

(28) Berkó, A.; Gubó, R.; Óvári, L.; Bugyi, L.; Szent, I.; Kónya, Z. Interaction of Rh with Rh Nanoparticles Encapsulated by Ordered Ultrathin TiO_{1+x} Film on $\text{TiO}_2(110)$ Surface. *Langmuir* **2013**, *29*, 15868–15877.

(29) Breinlich, C.; Buchholz, M.; Moors, M.; Le Moal, S.; Becker, C.; Wandelt, K. Scanning Tunneling Microscopy Investigation of Ultrathin Titanium Oxide Films Grown on $\text{Pt}_3\text{Ti}(111)$. *J. Phys. Chem. C* **2014**, *118*, 6186–6192.

(30) Óvári, L.; Berkó, A.; Gubó, R.; Rácz, Á.; Kónya, Z. Effect of a Gold Cover Layer on the Encapsulation of Rhodium by Titanium Oxides on Titanium Dioxide(110). *J. Phys. Chem. C* **2014**, *118*, 12340–12352.

(31) Gubó, R.; Óvári, L.; Kónya, Z.; Berkó, A. Growth of Gold on Pinwheel $\text{TiO}_{\sim 1.2}$ Encapsulation Film Prepared on Rhodium Nanocrystallites. *Langmuir* **2014**, *30*, 14545–14554.

(32) Giannozzi, P.; Baroni, S.; Bonini, N.; Calandra, M.; Car, R.; Cavazzoni, C.; Ceresoli, D.; Chiarotti, G. L.; Cococcioni, M.; Dabo, I.; et al. QUANTUM ESPRESSO: a Modular and Open-Source Software Project for Quantum Simulations of Materials. *J. Phys.: Condens. Matter* **2009**, *21*, 395502–395521.

(33) Vanderbilt, D. Soft Self-Consistent Pseudopotentials in a Generalized Eigenvalue Formalism. *Phys. Rev. B: Condens. Matter Mater. Phys.* **1990**, *41*, 7892–7895.

(34) Tersoff, J.; Hamann, D. R. Theory and Application for the Scanning Tunneling Microscope. *Phys. Rev. Lett.* **1983**, *50*, 1998–2001.

(35) Männig, A.; Zhao, Z.; Rosenthal, D.; Christmann, K.; Hoster, H.; Rauscher, H.; Behm, R. J. Structure and Growth of Ultrathin Titanium Oxide Films on $\text{Ru}(0001)$. *Surf. Sci.* **2005**, *576*, 29–44.

(36) Berkó, A.; Gubó, R.; Óvári, L.; Kónya, Z. Rh and Au Deposited on Ultrathin $\text{TiO}_{1.2}$ Film Formed on $\text{Rh}(111)$ Facets and the Effects of CO Exposure. *Surf. Sci.* **2015**, *641*, 300–304.

(37) Bugyi, L.; Szent, I.; Kónya, Z. Promotion and Inhibition Effects of TiO_x species on Rh Inverse Model Catalyst. *Appl. Surf. Sci.* **2014**, *313*, 432–439.

(38) Sedona, F.; Samb, M.; Artiglia, L.; Rizzi, G. A.; Vittadini, A.; Fortunelli, A.; Granozzi, G. Mobility of Au on TiO_x Substrates with Different Stoichiometry and Defectivity. *J. Phys. Chem. C* **2008**, *112*, 3187–3190.

(39) Cavaliere, E.; Kholmanov, I.; Gavioli, L.; Sedona, F.; Agnoli, S.; Granozzi, G.; Barcaro, G.; Fortunelli, A. Directed Assembly of Au and Fe Nanoparticles on a $\text{TiO}_x/\text{Pt}(111)$ Ultrathin Template: the Role of Oxygen Affinity. *Phys. Chem. Chem. Phys.* **2009**, *11*, 11305–11309.